Self-Injection Locked Frequency Conversion Laser

Jingwei Ling, Jeremy Staffa, Heming Wang, Boqiang Shen, Lin Chang, Usman A. Javid, Lue Wu, Zhiquan Yuan, Raymond Lopez-Rios, Mingxiao Li, Yang He, Bohan Li, John E. Bowers,* Kerry J. Vahala,* and Qiang Lin*

High-coherence visible and near-visible laser sources are centrally important to the operation of advanced position/navigation/timing systems as well as classical/quantum sensing systems. However, the complexity and size of these bench-top lasers are an impediment to their transition beyond the laboratory. Here, a system-on-chip that emits high-coherence near-visible lightwaves is demonstrated. The devices rely upon a new approach wherein wavelength conversion and coherence increase by self-injection locking are combined within a single nonlinear resonator. This simplified approach is demonstrated in a hybridly-integrated device and provides a short-term linewidth of around 4.7 kHz (10 kHz before filtering). On-chip converted optical power over 2 mW is also obtained. Moreover, measurements show that heterogeneous integration can result in a conversion efficiency higher than 25% with an output power over 11 mW. Because the approach uses mature III–V pump lasers in combination with thin-film lithium niobate, it can be scaled for low-cost manufacturing of high-coherence visible emitters. Also, the coherence generation process can be transferred to other frequency conversion processes, including optical parametric oscillation, sum/difference frequency generation, and third-harmonic generation.

1. Introduction

Highly coherent semiconductor lasers are crucial for many applications, ranging from communication, spectroscopy, metrology, medicine, to quantum technology. Recent advances in integrated photonic lasers via hybrid/heterogeneous integration have shown remarkably narrow linewidths that are now comparable to or even surplus the bench-top solid-state counterparts.[1–4] So far, the majority of research efforts have focused on the telecom band around 1.2–1.7 µm, primarily in response to the significant demand from optical communication. Development is fairly limited in the visible and near-infrared spectral regions where many important applications lie, such as classical/quantum sensing,[5] position/navigation /timing,[6] visible light communication,[7] 3D display,[8] virtual/augmented reality,[9] to name a few. A major challenge lies in that some wavelength ranges needed by related applications cannot be covered by current III–V gain media, which generally exhibit limited gain bandwidths in these spectral regions. Typical examples are optical atomic clocks[10] and quantum sensors,[5] which require either operation wavelengths or laser linewidths beyond the reach of current semiconductor lasers.

Optical frequency conversion based upon a quadratic optical nonlinearity is a powerful technology to transfer coherent laser radiation into new frequencies.[11–13] In recent years, the development of nonlinear photonic integrated circuits (PICs), particularly using the on-chip lithium-niobate-on-insulator (LNOI) platform,[14–29] has boosted nonlinear conversion efficiency while enabling photonic integration with active and passive waveguide elements. However, the coherence of an optical frequency conversion process is fundamentally constrained by the pumping light source due to the very nature of the underlying energy conversion of photons in the optical parametric interaction. Consequently, a high coherence of converted light imposes a stringent requirement on the narrow linewidth of the pump laser and/or sophisticated frequency stabilization to reference cavities,[13,30,31] which significantly increases the system complexity.[12,13,30–34]

Here we demonstrate for the first time, to the best of our knowledge, a hybridly integrated laser that produces efficient and ultra-coherent near-visible light. The device combines

J. Ling, M. Li, Y. He, Q. Lin
Department of Electrical and Computer Engineering
University of Rochester
Rochester, NY 14627, USA
E-mail: qiang.lin@rochester.edu
J. Staffa, U. A. Javid, R. Lopez-Rios, Q. Lin
Institute of Optics
University of Rochester
Rochester, NY 14627, USA
H. Wang, B. Shen, L. Wu, Z. Yuan, B. Li, K. J. Vahala
T. J. Watson Laboratory of Applied Physics
California Institute of Technology
Pasadena, CA 91125, USA
E-mail: vahala@caltech.edu
L. Chang, J. E. Bowers
Department of Electrical and Computer Engineering
University of California Santa Barbara
Santa Barbara, CA 93106, USA
E-mail: jbowers@ucsb.edu
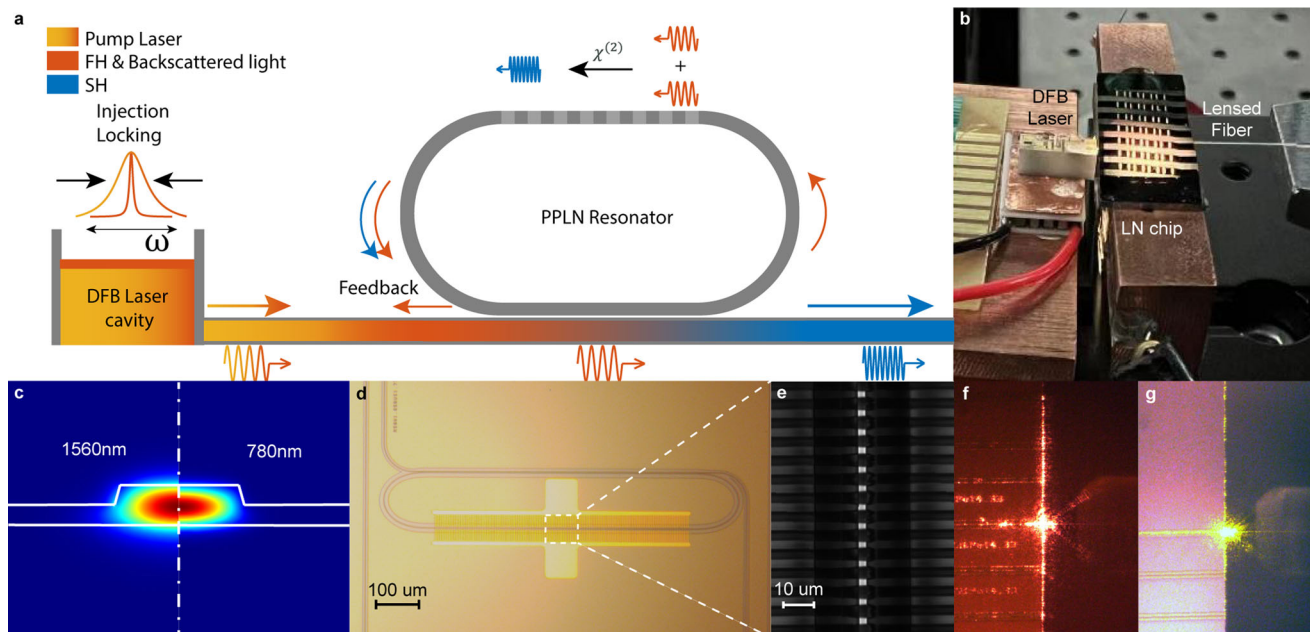
Figure 1. System concept, operating principle, and resonator structure. a) Conceptual diagram of the self-injection locking and second-harmonic generation process. b) Optical image of the self-injection-locked frequency-doubling chip system. c) Simulated optical mode field profile in the resonator waveguide for the fundamental quasi-TE$_{00}$ mode at 1560 nm (left) and at 780 nm (right). d) Optical image of the PPLN racetrack resonator. Dashed box gives region of grating imaged in panel (e). e) Second-harmonic confocal microscope image of the periodically poled waveguide section showing the uniformity of periodic poling. f,g) Optical images of the output facets of LN chips showing second harmonic emission generated at 780 nm (red) and 589 nm (yellow), respectively.
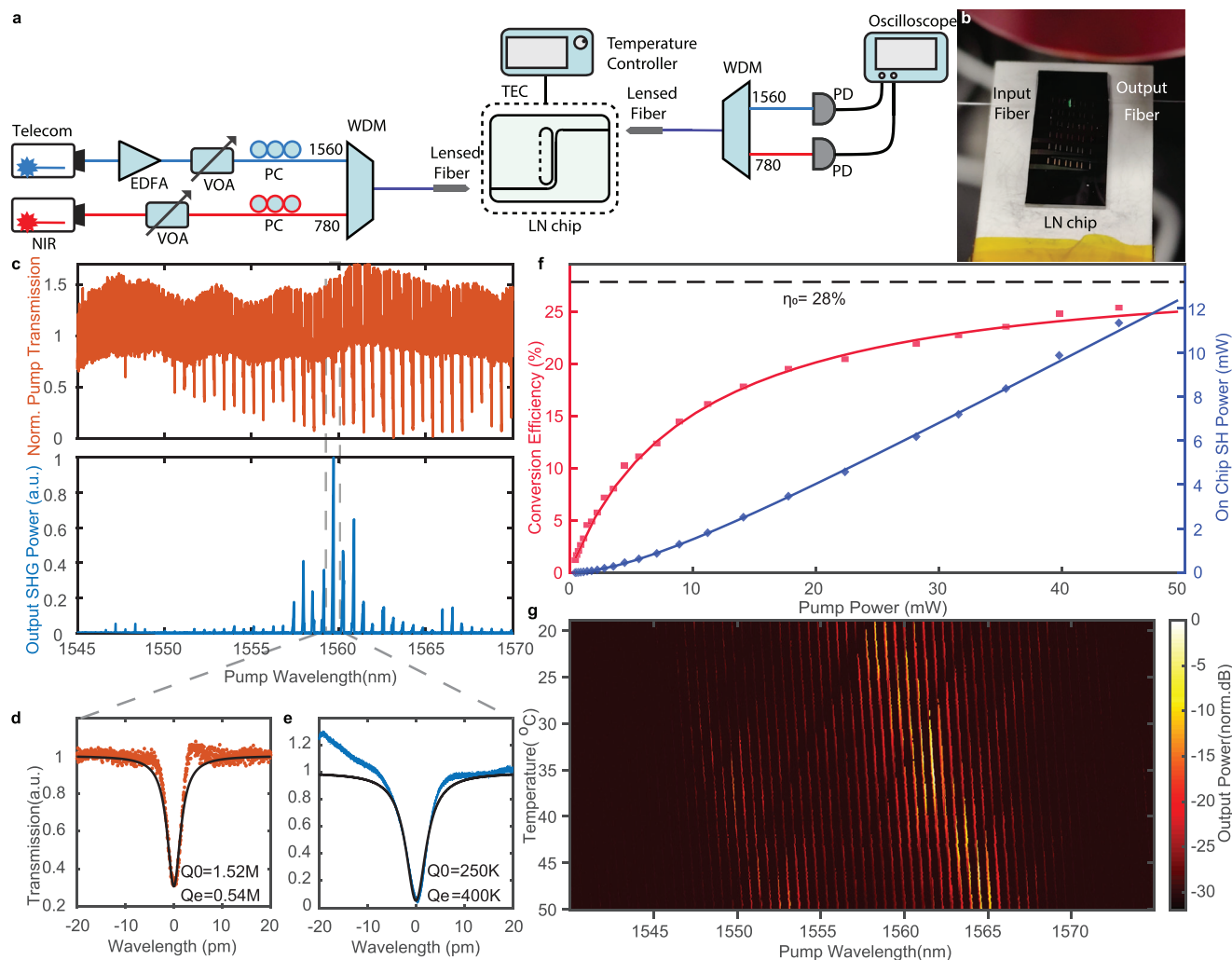
second harmonic generation (SHG) in an LNOI microresonator that also functions to line narrow a distributed-feedback (DFB) pumping laser through self-injection-locking (SIL).[4,35–38] This means that line narrowing and resonant enhancement for harmonic generation occur simultaneously, and also without the need for servo-control of the pumping laser for frequency tracking to the nonlinear resonator. With this fully integrated approach, we are able to produce highly coherent frequency-doubled light with a linewidth more than two orders of magnitude narrower than the pump laser itself. Such a chip-scale narrow-linewidth frequency conversion laser would offer tremendous advantages in size, weight, power, cost, functionality, and design flexibility of the laser wavelength via photonic integration, which would be indispensable for broad applications.

2. Device

The high-Q lithium niobate (LN) microresonator and DFB diode laser pump are facet-to-facet coupled as shown in **Figure 1**a,b. The LN resonator provides both resonantly enhanced SHG and feedback to line narrow the DFB pump. For the SHG function, it is periodically poled to quasi-phase match the doubly resonant pump and up-converted modes. For line narrowing, the high-Q mode that is pumped introduces weak backscattering into the DFB laser to achieve SIL. SIL has been shown to significantly enhance the coherence of telecom lasers,[4,38–41] including their application to soliton micro-comb generation.[42–44] With the near-instantaneous nature of the SHG process, the pump coherence is readily transferred to the up-converted light, resulting in narrow linewidth frequency-doubled light output.

We utilize a race-track LN microresonator fabricated on an *x*-cut LN-on-insulator platform. One of the straight waveguide sections is periodically poled for quasi phase-matching of SHG, while the other section is used for external coupling (Figure 1a). Such a coupling approach offers a rich set of external coupling conditions through the dispersive nature of straight-waveguide coupling, and the length of the coupling region is optimized to achieve the desired coupling condition for both SIL and SHG. An Euler curve[45] is adopted for the bending section of the race-track resonator to suppress the bending loss so as to achieve high intrinsic optical *Q*. The fundamental quasi-transverse-electric modes (TE$_{00}$ modes, Figure 1c) are utilized for SHG to take advantage of the largest tensor element of the nonlinear susceptibility, d_{33}, of LN. Here we target the SHG of a 1560 nm pump to a near-infrared wavelength near 780 nm, where narrow-linewidth is important for atomic clock, navigation, and quantum sensing applications based upon rubidium atoms.[5,10] The periodically poled section has a length of 630 µm and the resonator has a total cavity length of 1.9 mm, corresponding to a free-spectral range of 0.584 nm around the pump wavelength.

Figure 1d shows a fabricated device (see Experimental Section for fabrication details). The good uniformity of the periodic poling is shown in Figure 1e where a second-harmonic confocal microscope image is presented. Different facet coupling approaches are utilized for the fundamental pump input and SHG light output waveguides. The pump wave is coupled onto the chip with a 5 µm-wide taper designed for laser-to-chip facet coupling. The SHG light is coupled out of the chip to a lensed fiber using a 300-nm-wide inverse tapered waveguide. Figure 1f shows the 780 nm emission at the output facet with the lensed fiber

2200663 (2 of 7)

**ADVANCED
SCIENCE NEWS**

www.advancedsciencenews.com

www.lpr-journal.org

LASER
& PHOTONICS
REVIEWS

Figure 2. Characterization of the LN resonator properties and frequency-doubling performance. a) Experimental setup to characterize the linear optical properties and the SHG performance of the resonator device. EDFA, erbium-doped fiber amplifier; VOA, variable optical attenuator; PC, polarization controller; TEC, thermoelectric cooler; WDM, wavelength division multiplexer; PD, photodiode. b) Photograph of the LN chip showing lensed fiber coupling on both sides. c) Transmission spectrum (upper, red) and the corresponding generated second harmonic (lower, blue) when the continuous-wave laser is scanned from 1545 to 1570 nm. The device temperature is 20 °C. d,e) High resolution transmission spectrum of the pump resonance at 1559.5 nm (d) and the SHG resonance at 779.8 nm (e). The experimental data are shown as dots and the black solid curves show a fitting. f) SHG power (blue) and conversion efficiency (red) as a function of the pump power on chip. The pump wavelength is fixed at 1559.5 nm. The experimental data are shown as dots and the solid curves give the theoretical fitting from a depleted SHG theory (see Supporting Information). The dashed line indicates the theoretical maximum efficiency offered by the device. g) Temperature dependence of the laser-scanned second-harmonic generation spectrum (also see Figure 2c, lower panel, blue).

also visible in the image. To demonstrate the ability to precisely engineer other SHG wavelengths, another device was developed to produce SHG at 589 nm (an important wavelength for the operation of strontium clock systems). Yellow light emission at the output facet from this device is shown in Figure 1g. This device was not operated in the self-injection-locking mode on account of the lack of availability of a suitable DFB pumping laser.

3. Results

The device is first characterized by external pumping using a tunable laser (i.e., not SIL) and the experimental setup is shown in **Figure 2**a. A telecom pump laser (Santec TSL-510) and a

near-visible laser (New focus TLB-6700) characterize the linear properties of the resonator around the pump (1560 nm) and second-harmonic (780 nm) wavelengths. These are launched onto the chip via a lensed fiber (Figure 2b). To excite SHG, the telecom laser power is boosted by an erbium-doped fiber amplifier. The output of the chip is collected by another lensed fiber and then detected after the separation of the fundamental and harmonic signals. The fiber-chip coupling loss is measured to be 6.7 dB for the pump wave and 11 dB for the second harmonic light. The device temperature is controlled by a thermo-electric cooler (TEC) to tune the phase-matching wavelength. Figure 2c (upper panel) shows the transmission spectrum of the device in the telecom band, the background oscillation comes from
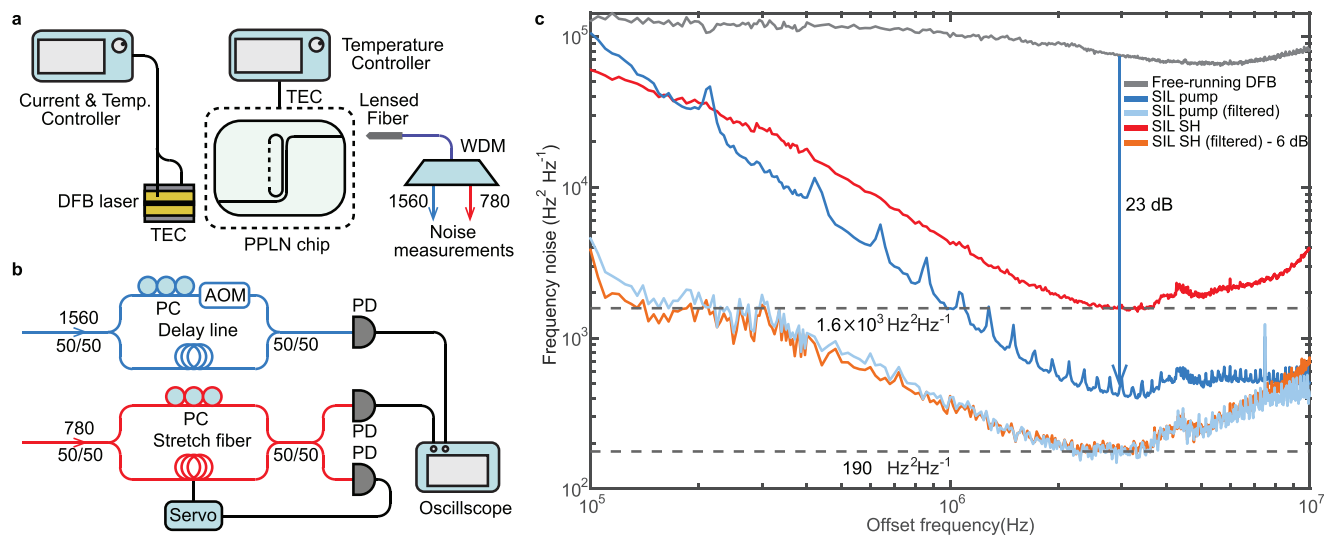
Figure 3. Self-injection-locked SHG lasing operation and experimental setup for linewidth characterization. a) Experimental setup for SIL frequency doubling. b) Frequency noise measurement setups for the SIL pump laser and the second harmonic light. AOM, acoustic-optical modulator. c) Recorded frequency noise spectrum. Gray, blue, and red traces show the frequency noise spectrum of the free-running DFB laser, SIL pump laser, and SIL frequency-doubled light, respectively. The light blue trace and the orange traces show the frequency noise of the pump light and 6 dB down-shifted SHG light when frequency jumping noise is removed from data.

waveguide facet reflection. The resonator modes exhibit a range of coupling conditions from under coupled to over coupled. For pump wavelengths around ≈1560 nm, the device is designed to be over-coupled but with sufficient loaded Q so as to enable strong SIL while still providing relatively high SHG efficiency. As shown in Figure 2d, a pump resonance at 1559.5 nm exhibits an intrinsic optical Q of $Q_{1,0} = 1.52 \times 10^6$, which is slightly over-coupled with an external coupling Q of $Q_{1,e} = 5.4 \times 10^5$. A corresponding SHG resonance at 779.8 nm exhibits an intrinsic optical Q of $Q_{2,0} = 2.5 \times 10^5$ and an external coupling Q of $Q_{2,e} = 4 \times 10^5$, as shown in Figure 2e. Figure 2c (lower panel) gives the SHG light generated upon spectral scan.

Maximum conversion occurs at the pump wavelength of 1559.5 nm. By fixing the laser wavelength at this resonance the SHG output power versus coupled power is measured in Figure 2f. The power of the SHG light increases quadratically with the pump power at low pump power with a slope efficiency of 3000% W^{-1}. At higher pump power, there is a linear dependence. Maximum SHG power is 11.3 mW at a pump power of 44.6 mW, corresponding to a conversion efficiency of about 25%. This conversion efficiency is among the highest reported to date for on-chip LN devices.[18,23,27,28] The measurements are in good agreement with the theory (solid curves), which predicts a maximum conversion efficiency of 28%. It was observed that optimal phase matching depended upon pumping power, through the photorefractive effect. This, in turn, required the temperature to be adjusted at each pumping power so as to maximize power conversion (see Section 4). This was also necessary in the SIL measurements discussed below. The use of magnesium-doped LN material could potentially reduce or eliminate this procedure in the future.

The phase-matched SHG wavelength can be tuned thermo-optically as shown in Figure 2g. Within a small temperature range (say, 20–25 °C), the SHG conversion maximum remains

within the same resonance and features a tuning slope of 39 pm K^{-1} and a continuous tuning range of over 0.2 nm, which is primarily induced by the temperature dependence of refractive index. When the device temperature increases beyond this range, the dominant SHG peak switches to a nearby mode. This is induced by the dispersion of phase matching condition, as caused by differences in the thermo-optic coefficient of LN at pump and SHG wavelengths, and by the first order dispersion of resonances. The resulting tuning range of ≈7 nm over 30K (tuning slope of about 0.23 nm K^{-1}) is useful for self-injection locking since it enables matching of the pump resonance wavelength to emission of the DFB laser.

For SIL frequency doubling, the setup at the input end is replaced by a DFB laser (Freedom Photonics), with direct facet-to-facet coupling to the LN chip as shown in **Figure 3**a and Figure 1b. The laser and the LN chip are mounted on translation stages with piezoelectric controllers. This allows precise alignment of the optical ports as well as control of the micron-scale gap between laser and chip (to set the feedback phase of the SIL process). The laser temperature is adjusted so that the output wavelength of the DFB laser roughly matches the phase-matching wavelength (1559.5 nm), and the laser current is increased to engage injection locking. At maximum pump current, the estimated on-chip pump power is 12 mW and the corresponding on-chip SHG power is 2 mW, consistent with Figure 2f.

The frequency noise of the self-injection locked pump laser is characterized with a self-heterodyne approach[46] while the noise of SHG light is measured with a conventional homodyne detection setup with quadrature-point locking[47] (shown in Figure 3b; see Experimental Section). The results are shown in Figure 3c. The high-offset-frequency pump noise is significantly reduced compared to the free-running DFB laser by over 20 dB, demonstrating the effect of the SIL process. The SHG noise reaches a level of 1600 Hz² Hz^{-1} at around 3 MHz offset frequency. The

slight rise in this noise toward higher offset frequencies is not understood, but is not observed in another device whose test results are presented in the Supporting Information. These data place the SHG short-term linewidth in the range of 10–30 kHz. Much larger noise suppression factors (50–60 dB) are expected if the LN resonator Q factor can be boosted to material limits reported recently.[48]

At low offset frequencies, the frequency noise is observed to increase and is shown in the Supporting Information to be caused by small, random-in-time frequency jumps of the SIL laser. A further study of the jumps is presented in the Supporting Information, including a method to isolate the jumps that enables study of their statistics as well as filtering from the frequency noise spectra. Such filtered noise spectra for the pump and the SHG signal are presented in Figure 3c. The origin of the frequency jumps is not currently understood.

Because the SHG process entails squaring of the pumping field, the SHG field contains exactly twice the temporal pump phase-noise fluctuation. Since the frequency noise spectrum is computed from the variance of this phase noise fluctuation, the SHG frequency noise must therefore be 4× larger (6 dB) than the pump frequency noise. To verify this effect, the filtered SHG frequency noise data shifted by 6 dB is included in Figure 3c, and shows good agreement with the filtered pump frequency noise data. As the two traces are measured using independent setups with different working principles, this further validates the noise-related physics associated with the second-harmonic process. Figure 3c shows that the SHG noise reaches a level of 760 Hz^2 Hz^{-1} ($= 4 \times 190$ Hz^2 Hz^{-1}) that corresponds to a short-term linewidth of 4.7 kHz. As an aside, the unfiltered SHG frequency noise in Figure 3c would also show closer agreement (once shifted by 6 dB) with the unfiltered pump frequency noise if not for a technical issue associated with measuring this noise in the presence of the frequency jumps. This is verified in the Supporting Information.

4. Discussion

The device presented here exhibits a resonator coupling ratio of $\frac{Q_0}{Q_e} = 2.8$ at the fundamental pump mode. Modeling shows that a similar level of over-coupling at the SHG mode can boost the conversion efficiency to above 50%. Also, the laser-to-chip coupling loss in the current device is relatively high, and the linewidth of the SHG light can be further improved by reducing the laser-to-chip coupling loss using a better waveguide taper design. High coupling loss could also play a role in the observed low-frequency noise behavior. Possible connection of this noise to the photo-refractive effect through mechanisms such as Barkhausen noise[49] is also under investigation. For example, switching to an MgO-doped LNOI wafer platform is being studied to significantly reduce the photorefractive effect.[50] And any impact this has on the observed noise will be tested.

Both the SHG process and the SIL mechanism benefit from a resonator with a high intrinsic optical Q, which would allow strong over-coupling for efficient SHG while simultaneously providing a high loaded optical Q for strong SIL. Intrinsic optical Q as high as 10^8 has recently been demonstrated in on-chip LN microresonators.[48] This value of optical Q is expected to further

suppress the short-term linewidth of the frequency-doubled laser down to ≈10-Hz level.

In summary, we have demonstrated a highly efficient chip-scale laser that produces high-coherence near-visible light by combining self-injection locking and second-harmonic generation within a single high-Q nonlinear resonator, with the capability to migrate easily to other wavelengths. A near-visible linewidth as narrow as 4.7 kHz (10 kHz before filtering) is achieved by suppression of pump frequency noise. Also, on-chip converted power over 2 mW is obtained in a hybrid-integrated design. Separate measurements using an external pump laser yield a maximum conversion efficiency over 25% and a maximum SHG power of 11.3 mW. These measurements suggest that much higher integrated device performance will be possible by replacing the current hybrid design with a heterogeneously integrated device that features low pump to LN resonator coupling loss.

The demonstrated approach can be applied to other optical frequency conversion processes, such as optical parametric oscillation for frequency down-conversion and third-harmonic generation for up-conversion to shorter wavelengths. Moreover, the on-chip LN platform enables integration with electro-optic components for further functional enhancement. A highly coherent, chip-scale visible/near-visible optical source can profoundly impact many applications, including optical clocks, metrology, navigation, sensing, and quantum information processing.[6,7,10]

5. Experimental Section

Device Fabrication: The device was fabricated on a congruent *x*-cut thin film LNOI wafer, with 600 nm LN sitting upon a 4.7 μm silica layer. ZEP-520A resist was used as the mask for a first e-beam lithography step (EBL), followed by 300 nm Ar-ion milling to define the waveguide. Next, a second EBL writing step was performed on PMMA resist, and 400 nm electrodes were created using a gold evaporation and lift-off process. A 3 μm separation was introduced between the electrodes and the waveguide to reduce the absorption. Finally, the chip was diced and polished to acquire good fiber-to-chip and laser-to-chip coupling.

The periodic poling process was similar to the previously reported methods,[25] but the poling was done after the etching process. Several pulses of 10 ms duration and voltage of 240 V were applied with the electric field along the negative *z*-axis of the LN crystal. The SHG power was monitored during poling until SHG power was maximized. The number of pulses used were around 20, and the poling uniformity can be clearly observed in Figure 1e. A poling period of 4.3 μm was used to compensate for the momentum mismatch between the pump and SHG in the 1.75 μm waveguide.

DFB Laser: The pump laser used in this work was an InP DFB laser as shown in Figure 3a. It had high-reflection coatings on the back facet and anti-reflection coatings on the front facet. The threshold current was 50 mA, and the total output power of the laser could reach more than 100 mW under 400 mA pumping current. The slope efficiency of the laser was around 0.28 mW mA^{-1} and the peak wall-plug efficiency could reach 20%. The lasing was single-mode and its wavelength also shifted from 1558.2 to 1560.2 nm with increasing bias current (about -0.75 GHz mA^{-1}). The laser chip was mounted on a sub-mount with a thermoelectric cooler underneath. The temperature of the laser diode could be controlled within 1 mK.

Noise Measurements: The self-injection-locked laser pump at 1559.5 nm was characterized by a self-heterodyne method (see Figure 3b upper branch in blue). A portion of the laser was frequency-downshifted by an AOM and recombined with another portion delayed by a 1-km-long fiber. The optical signal was received by a balanced photodetector, converted to a radio-frequency signal, and recorded with a high-speed

oscilloscope. Phase fluctuations were extracted using Hilbert transforms and then converted to frequency fluctuation through time-domain difference. Other details of the setup are documented elsewhere.[51]

The second harmonic light at 779.8 nm was characterized by a homodyne method (see Figure 3b lower branch in red). The homodyne method (as opposed to the heterodyne method describe above) was used at 779.8 nm, because existing AOM optical losses at this wavelength were too large. The system was stabilized around the quadrature point using a servo loop to control a stretched optical fiber, such that phase fluctuation could be linearly converted to voltage. Compared to the self-heterodyne method, the laser was not frequency-shifted, and the stretch fiber was equivalent to a 15 m delay. The output signal was sent to the same oscilloscope for data recording, which was synchronized with the pump laser signal for comparison. Phase fluctuations could be calculated by normalizing the signal against the voltage swing, measured separately by applying a sweeping signal at the stretch fiber. Other details of the calculation are documented elsewhere.[47]

Supporting Information

Supporting Information is available from the Wiley Online Library or from the author.

Conflict of Interest

The authors declare no conflict of interest.

Author Contributions

J.L., J.S., H.W., B.S., and L.C. contributed equally to this work. J.L., J.S., B.Q., H.W., L.C., J.B., K.V., and Q.L. conceived the experiment. J.L. and J.S designed and fabricated the PPLN device, and L.C. designed and fabricated the DFB laser. J.L., J.S., B.Q., and H.W. carried out the device characterization. U.J., L.W., and M.L. assisted in the device fabrication. U.J., R.L., Y.H., and Z.Y. assisted in experiments. J.L., J.S., B.Q., H.W., L.C., and Q.L. wrote the manuscript with contribution from all authors. Q.L., K.V., and J.B. supervised the project.

Data Availability Statement

The data that support the findings of this study are available from the corresponding author upon reasonable request.

[1] M. A. Tran, D. Huang, J. E. Bowers, *APL Photonics* **2019**, *4*, 111101.
[2] D. Huang, M. A. Tran, J. Guo, J. Peters, T. Komljenovic, A. Malik, P. A. Morton, J. E. Bowers, *Optica* **2019**, *6*, 745.
[3] Y. Fan, A. van Rees, P. J. Van der Slot, J. Mak, R. M. Oldenbeuving, M. Hoekman, D. Geskus, C. G. Roeloffzen, K.-J. Boller, *Opt. Express* **2020**, *28*, 21713.
[4] W. Jin, Q.-F. Yang, L. Chang, B. Shen, H. Wang, M. A. Leal, L. Wu, M. Gao, A. Feshali, M. Paniccia, K. J. Vahala, J. E. Bowers, *Nat. Photonics* **2021**, *15*, 346.
[5] C. L. Degen, F. Reinhard, P. Cappellaro, *Rev. Mod. Phys.* **2017**, *89*, 035002.
[6] R. Lutwak, in *2014 Int. Symp. on Inertial Sensors and Systems (ISISS)*, IEEE, Piscataway, NJ **2014**, pp. 1–4.
[7] P. H. Pathak, X. Feng, P. Hu, P. Mohapatra, *IEEE Commun. Surv. Tutorials* **2015**, *17*, 2047.
[8] K. V. Chellappan, E. Erden, H. Urey, *Appl. Opt.* **2010**, *49*, F79.
[9] J. Xiong, E.-L. Hsiang, Z. He, T. Zhan, S.-T. Wu, *Light: Sci. Appl.* **2021**, *10*, 216.
[10] A. D. Ludlow, M. M. Boyd, J. Ye, E. Peik, P. O. Schmidt, *Rev. Mod. Phys.* **2015**, *87*, 637.
[11] M. M. Fejer, *Phys. Today* **1994**, *47*, 25.
[12] M. H. Dunn, M. Ebrahimzadeh, *Science* **1999**, *286*, 1513.
[13] M. Ebrahim-Zadeh, in *Handbook of Optics*, Vol. *4*, McGraw-Hill, New York **2010**, Ch. 17, pp. 1–33.
[14] A. Boes, B. Corcoran, L. Chang, J. Bowers, A. Mitchell, *Laser Photonics Rev.* **2018**, *12*, 1700256.
[15] D. Zhu, L. Shao, M. Yu, R. Cheng, B. Desiatov, C. Xin, Y. Hu, J. Holzgrafe, S. Ghosh, A. Shams-Ansari, E. Puma, N. Sinclair, C. Reimer, M. Zhang, M. Loncar, *Adv. Opt. Photonics* **2021**, *13*, 242.
[16] L. Chang, Y. Li, N. Volet, L. Wang, J. Peters, J. E. Bowers, *Optica* **2016**, *3*, 531.
[17] R. Wolf, Y. Jia, S. Bonaus, C. S. Werner, S. J. Herr, I. Breunig, K. Buse, H. Zappe, *Optica* **2018**, *5*, 872.
[18] C. Wang, C. Langrock, A. Marandi, M. Jankowski, M. Zhang, B. Desiatov, M. M. Fejer, M. Lončar, *Optica* **2018**, *5*, 1438.
[19] R. Luo, Y. He, H. Liang, M. Li, J. Ling, Q. Lin, *Phys. Rev. Appl.* **2019**, *11*, 034026.
[20] J. Lin, N. Yao, Z. Hao, J. Zhang, W. Mao, M. Wang, W. Chu, R. Wu, Z. Fang, L. Qiao, W. Fang, Y. Bo, Y. Cheng, *Phys. Rev. Lett.* **2019**, *122*, 173903.
[21] A. Rao, K. Abdelsalam, T. Sjaardema, A. Honardoost, G. F. Camacho-Gonzalez, S. Fathpour, *Opt. Express* **2019**, *27*, 25920.
[22] J.-Y. Chen, Z.-H. Ma, Y. M. Sua, Z. Li, C. Tang, Y.-P. Huang, *Optica* **2019**, *6*, 1244.
[23] J. Lu, J. B. Surya, X. Liu, A. W. Bruch, Z. Gong, Y. Xu, H. X. Tang, *Optica* **2019**, *6*, 1455.
[24] Y. Niu, C. Lin, X. Liu, Y. Chen, X. Hu, Y. Zhang, X. Cai, Y.-X. Gong, Z. Xie, S. Zhu, *Appl. Phys. Lett.* **2020**, *116*, 101104.
[25] J. Zhao, M. Rüsing, U. A. Javid, J. Ling, M. Li, Q. Lin, S. Mookherjea, *Opt. Express* **2020**, *28*, 19669.
[26] J. Lu, M. Li, C.-L. Zou, A. Al Sayem, H. X. Tang, *Optica* **2020**, *7*, 1654.
[27] T. P. McKenna, H. S. Stokowski, V. Ansari, J. Mishra, M. Jankowski, C. J. Sarabalis, J. F. Herrmann, C. Langrock, M. M. Fejer, A. H. Safavi-Naeini, *arXiv:2102.05617*, **2021**.
[28] J.-Y. Chen, C. Tang, M. Jin, Z. Li, Z. Ma, H. Fan, S. Kumar, Y. M. Sua, Y.-P. Huang, *Laser Photonics Rev.* **2021**, *15*, 2100091.
[29] L. Wang, X. Zhang, F. Chen, *Laser Photonics Rev.* **2021**, *15*, 2100409.
[30] I. Ricciardi, S. Mosca, M. Parisi, P. Maddaloni, L. Santamaria, P. De Natale, M. De Rosa, *Opt. Lett.* **2015**, *40*, 4743.
[31] A. Ly, C. Siour, F. Bretenaker, *Opt. Express* **2017**, *25*, 9049.
[32] R. L. Byer, *Science* **1988**, *239*, 742.
[33] C. Czeranowsky, E. Heumann, G. Huber, *Opt. Lett.* **2003**, *28*, 432.

**ADVANCED
SCIENCE NEWS**

www.advancedsciencenews.com

**LASER
& PHOTONICS
REVIEWS**

www.lpr-journal.org

[34] L. Taylor, Y. Feng, D. B. Calia, *Opt. Express* **2009**, *17*, 14687.

[35] B. Dahmani, L. Hollberg, R. Drullinger, *Opt. Lett.* **1987**, *12*, 876.

[36] H. Li, N. Abraham, *IEEE J. Quantum Electron.* **1989**, *25*, 1782.

[37] D. R. Hjelme, A. R. Mickelson, R. G. Beausoleil, *IEEE J. Quantum Electron.* **1991**, *27*, 352.

[38] B. Li, W. Jin, L. Wu, L. Chang, H. Wang, B. Shen, Z. Yuan, A. Feshali, M. Paniccia, K. J. Vahala, J. E. Bowers, *Opt. Lett.* **2021**, *46*, 5201.

[39] W. Liang, V. Ilchenko, D. Eliyahu, A. Savchenkov, A. Matsko, D. Seidel, L. Maleki, *Nat. Commun.* **2015**, *6*, 7957.

[40] N. Kondratiev, V. Lobanov, A. Cherenkov, A. Voloshin, N. Pavlov, S. Koptyaev, M. Gorodetsky, *Opt. Express* **2017**, *25*, 28167.

[41] G. Lihachev, J. Riemensberger, W. Weng, J. Liu, H. Tian, A. Siddharth, V. Snigirev, R. N. Wang, J. He, S. A. Bhave, T. J. Kippenberg, *arXiv:2104.02990*, **2021**.

[42] B. Shen, L. Chang, J. Liu, H. Wang, Q.-F. Yang, C. Xiang, R. N. Wang, J. He, T. Liu, W. Xie, J. Guo, D. Kinghorn, L. Wu, Q.-X. Ji, T. J Kippenberg, K. Vahala, J. E. Bowers, *Nature* **2020**, *582*, 365.

[43] A. S. Voloshin, N. M. Kondratiev, G. V. Lihachev, J. Liu, V. E. Lobanov, N. Y. Dmitriev, W. Weng, T. J. Kippenberg, I. A. Bilenko, *Nat. Commun.* **2021**, *12*, 1.

[44] C. Xiang, J. Liu, J. Guo, L. Chang, R. N. Wang, W. Weng, J. Peters, W. Xie, Z. Zhang, J. Riemensberger, J. Selvidge, T. J. Kippenberg, J. E. Bowers, *Science* **2021**, *373*, 99.

[45] L. Zhang, L. Jie, M. Zhang, Y. Wang, Y. Xie, Y. Shi, D. Dai, *Photonics Res.* **2020**, *8*, 684.

[46] S. Camatel, V. Ferrero, *J. Lightwave Technol.* **2008**, *26*, 3048.

[47] H. Lee, T. Chen, J. Li, K. Y. Yang, S. Jeon, O. Painter, K. J. Vahala, *Nat. Photonics* **2012**, *6*, 369.

[48] R. Gao, N. Yao, J. Guan, L. Deng, J. Lin, M. Wang, L. Qiao, W. Fang, Y. Cheng, *Chin. Opt. Lett.* **2022**, *20*, 011902.

[49] A. S. Kewitsch, A. Saito, A. Yariv, M. Segev, R. R. Neurgaonkar, *J. Opt. Soc. Am. B* **1995**, *12*, 1460.

[50] Y. Furukawa, K. Kitamura, S. Takekawa, A. Miyamoto, M. Terao, N. Suda, *Appl. Phys. Lett.* **2000**, *77*, 2494.

[51] H. Wang, L. Wu, Z. Yuan, K. Vahala, *arXiv:2010.09248*, **2020**.

2200663 (7 of 7)